buildings

MDPI

Article

A Beam-Deflection-Based Approach for Cable Damage Identification

Yanxiao Yang [1,2], Lin Li [1], Sha Li [3,*], Li Zhao [4,*], Hongbin Xu [5,6,*], Weile Yang [7], Shaopeng Zhang [8,9] and Meng Wang [10]

1 School of Art and Design, Shijiazhuang University, Shijiazhuang 050035, China; 2508014@sjzc.edu.cn (Y.Y.); libant1006@163.com (L.L.)
2 School of Civil Engineering, Shijiazhuang Tiedao University, Shijiazhuang 050043, China
3 School of Civil Engineering and Architecture, Hebei University of Engineering Science, Shijiazhuang 050091, China
4 Hebei Vocational College of Labour Relations, Shijiazhuang 050093, China
5 Optoelectronic System Laboratory, Institute of Semiconductors, Chinese Academy of Sciences, Beijing 100083, China
6 National Key Laboratory of Green and Long-Life Road Engineering in Extreme Environment, Shenzhen University, Shenzhen 518060, China
7 China First Highway Engineering Co., Ltd., Beijing 100024, China; weileyang1986@163.com
8 Civil Engineering Design Research Institute, China Railway Design Corporation, Tianjin 300142, China; zhangshaopeng@crdc.com
9 School of Civil Engineering, Guangzhou University, Guangzhou 510006, China
10 Hebei Coal Science Research Institute Co., Ltd., Xingtai 054000, China; hbwm1986@163.com
* Correspondence: lisha20250928@163.com (S.L.); zl201987@163.com (L.Z.); xuhongbin@semi.ac.cn (H.X.); Tel.: +86-17731919060 (S.L.); +86-13303011159 (L.Z.); +86-15833113800 (H.X.)

Abstract

To address the limitations of existing cable damage identification methods in terms of environmental robustness and measurement dependency, this study proposes a novel damage identification approach based on the second-order difference characteristics of main beam deflection. Through theoretical derivation, the intrinsic relationship between cable damage and local deflection field disturbances in the main beam was revealed, leading to the innovative definition of a second-order difference of deflection (DISOD) index for damage localization. By analyzing the second-order deflection differences at the anchorage points of a three-cable group (a central cable and its two adjacent cables), the damage status of the central cable can be directly determined. The research comprehensively employed finite element numerical simulations and scaled model experiments to systematically validate the method's effectiveness in identifying single-cable and double-cable (both adjacent and non-adjacent) damage scenarios under various noise conditions. This method enables damage localization without direct cable force measurement, demonstrates anti-noise interference capability, achieves rapid and accurate identification, and provides a technically promising solution for the health monitoring of long-span cable-stayed bridges.

Keywords: stay cable; damage identification; second-order difference of deflection; cable force; bending moment

Check for updates

Academic Editor: Shaohong Cheng

Received: 3 December 2025
Revised: 29 December 2025
Accepted: 30 December 2025
Published: 8 January 2026

Copyright: © 2026 by the authors. Licensee MDPI, Basel, Switzerland. This article is an open access article distributed under the terms and conditions of the Creative Commons Attribution (CC BY) license.

1. Introduction

Stay cables, as the primary load-bearing components of cable-stayed bridges, are particularly susceptible to environmental corrosion and dynamic loads over their operational lifespan, leading to various types of damage such as strand breakage, surface degradation,

and structural impairments. Surface deterioration typically presents as aging and cracking of the protective coating surrounding the cable, while structural issues may include broken strands, corrosion, anchorage loss, and fatigue failure induced by vehicular traffic, among other factors [1–3]. These types of damage can compromise cable tension, impacting the alignment of the main beam and posing significant safety risks to bridge operations. As a result, the accurate assessment of stay cable condition, timely detection of damage, and decision-making regarding cable replacement have remained critical priorities in the global bridge engineering community. Therefore, the development of effective inspection techniques and maintenance strategies is of paramount importance to ensure the ongoing safe and reliable operation of cable-stayed bridges.

Currently, common cable damage detection methods include direct inspection methods and indirect methods based on dynamic responses, as well as methods based on static parameters. Direct inspection methods encompass visual inspection, ultrasonic testing, and magnetic flux leakage techniques. Among these, visual inspection is the most widely applied method in annual bridge inspections; however, it has the drawbacks of being time-consuming, labor-intensive, and potentially dangerous, and the results largely depend on the inspector's experience and professional skills [4]. Ultrasonic methods require the prior placement of acoustic emission sensors [5], while magnetic flux leakage techniques demand complex equipment and the leakage signal can be easily affected by the protective casing, thereby impacting the accuracy of damage identification [6–8]. Indirect damage identification methods based on the bridge's dynamic response include modal frequency [9], modal shapes, flexibility curvature [10–12], acceleration, curvature modes [13], modal strain energy, and acceleration, among other parameters. Modal shapes are liner results. Damage is a nonlinear phenomenon and generally shows up first in higher frequencies. By the time changes in lower mode shapes occur too much damage may have occurred. However, due to the dynamic response of bridges being easily affected by external environments, the complexity of actual bridge structures and outdoor conditions, as well as the incompleteness of the measured data, the uncertainty of the structural dynamic response is relatively large, and the practical application of existing research results still requires improvement. In addition, methods for identifying cable damage based on static parameters (such as temperature deflections) are also gaining attention [14].

In contrast to the dynamic responses observed in the structure, the deflection response signal of a bridge stands out for its remarkable stability. Static parameter methods have piqued researcher interest due to their minimal environmental impact. Cable damage can alter tension, allowing for identification through tension variations. Practical engineering methods, such as hydraulic jacks and pressure sensors, are commonly used, but their accuracy may be compromised by external factors, leading to reduced repeatability of results.

Wang et al. [15,16] and other researchers have focused on different aspects of bridge structures, proposing methods to identify damaged components through careful analysis of deflection differences and cable force changes. These methods have been validated through laboratory experiments, showcasing their accuracy and reliability.

Yang et al. [17] proposed a cable damage identification method based on the flexibility matrix of local beam segments. This method identifies changes in cable forces within the region by establishing the relationship between the flexibility matrix of local beam segments and variations in cable forces, thereby enabling the localization of damaged cables. However, the selection of the length of the local beam segment has a significant impact on the identification results: inappropriate length may lead to a decrease in the accuracy of cable damage localization or even misjudgment.

Shu [18] innovatively introduced a method for the inverse calculation of cable force in cable-stayed bridges, leveraging the correlation between the main beam deflection and cable force. By integrating this with the inherent mechanical properties of the cable-stayed cables, he also developed a dynamic approach to quantitatively assess damages to the cables in real-time.

An innovative strategy for identifying cable damage is introduced in this work, utilizing second-order difference analysis of beam deflection. By examining the evolving patterns of large-scale deformation features, the method addresses a fundamental constraint of conventional approaches—their susceptibility to environmental variations. This research pioneers an inverse analytical route linking global structural deformation to localized damage states. The framework offers a mechanics-based interpretation model for assessing cable integrity in long-span cable-supported bridges, while simultaneously delivering a cost-efficient monitoring system with minimal hardware requirements and enhanced resilience to field conditions. The proposed methodology shows considerable promise for implementation in real-world engineering environments.

2. Materials and Methods

2.1. Theory of Damage Identification for Stay Cables

2.1.1. Relationship Between Cable Tension and Second Derivative of Deflection

(1) Relationship between Bending Moment and External Load on a Local Beam Section

Consider a local segment AB extracted from the main girder of a cable-stayed bridge. This segment is subjected to a uniformly distributed load and the vertical components of the forces from the stay cables, as illustrated in Figure 1. The vertical components of the forces exerted by the individual stay cables along the segment, arranged from left to right, are respectively denoted as $Y_1, \ldots, Y_{k-1}, Y_k, Y_{k+1}, \ldots, Y_m$.

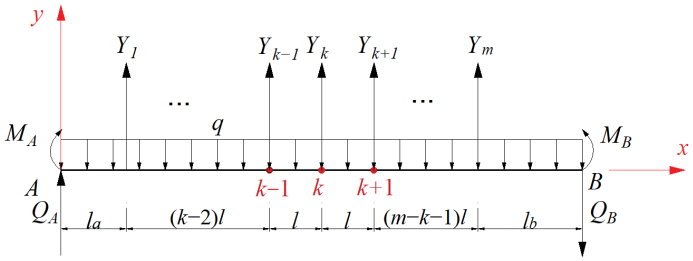


Figure 1. Force analysis of local beam segment AB.

The bending moments at cable anchorage points $k-1$, k, and $k+1$ can be expressed as:

$$\begin{cases} M_{k-1} = M_{k-1}^E + M_{k-1}^Q + M_{k-1}^F \\ M_k = M_k^E + M_k^Q + M_k^F \\ M_{k+1} = M_{k+1}^E + M_{k+1}^Q + M_{k+1}^F \end{cases} \quad (1)$$

where

M_{k-1}^E, M_{k-1}^Q and M_{k-1}^F represent the bending moments at point $k-1$ induced by the support reactions, uniformly distributed load q, and all concentrated loads, respectively;

M_k^E, M_k^Q and M_k^F denote the bending moments at point k caused by the support reactions, uniformly distributed load q, and all concentrated loads, respectively;

M_{k+1}^E, M_{k+1}^Q and M_{k+1}^F indicate the bending moments at point $k+1$ generated by the support reactions, uniformly distributed load q, and all concentrated loads, respectively.

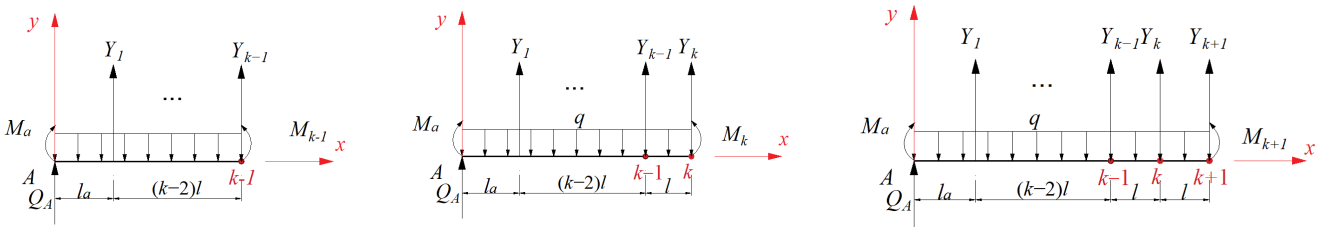
Definition:

$$M^R = M_k - \frac{1}{2}(M_{k-1} + M_{k+1}) \tag{2}$$

Substituting Equation (1) into Equation (2) yields:

$$M^R = (M_k^E + M_k^Q + M_k^F) - \frac{1}{2}\left(\left(M_{k-1}^E + M_{k-1}^Q + M_{k-1}^F\right) + \left(M_{k+1}^E + M_{k+1}^Q + M_{k+1}^F\right)\right) \tag{3}$$

By considering the left−hand segments of sections $k-1$, k, and $k+1$ in Figure 1 as free bodies, the mechanical model is obtained as shown in Figure 2.



(**a**) A−K − 1 (**b**) A−K (**c**) A−K + 1

Figure 2. Force analysis of isolated body.

Based on the equilibrium conditions, the bending moments generated by the support reactions at points $k-1$, k, and $k+1$ of the beam segment are:

$$\begin{cases} M_{k-1}^E = M_a + Q_a(l_a + (k-2)l) \\ M_k^E = M_a + Q_a(l_a + (k-2)l + l) \\ M_{k+1}^E = M_a + Q_a(l_a + (k-2)l + 2l) \end{cases} \tag{4}$$

Based on the equilibrium conditions, the bending moments generated by the uniformly distributed loads at points $k-1$, k, and $k+1$ of the beam segment are:

$$\begin{cases} M_{k-1}^Q = -\frac{q(l_a+(k-2)l)^2}{2} \\ M_k^Q = -\frac{q(l_a+(k-2)l+l)^2}{2} \\ M_{k+1}^Q = -\frac{q(l_a+(k-2)l+2l)^2}{2} \end{cases} \tag{5}$$

The bending moments induced by all cable forces at sections $k-1$, k, and $k+1$ of the beam segment are:

$$\begin{cases} M_{k-1}^F = \sum_{j=1}^{k-2} Y_j(k-j-1)l \\ M_k^F = \sum_{j=1}^{k-1} Y_j(k-j)l \\ M_{k+1}^F = \sum_{j=1}^{k} Y_j(k-j+1)l \end{cases} \tag{6}$$

Substituting Equations (4)–(6) into Equation (3) yields:

$$M^R = \frac{1}{2}ql^2 - \frac{1}{2}Y_k l \tag{7}$$

(2) Relationship Between Bending Moment and Deflection in Local Beam Sections

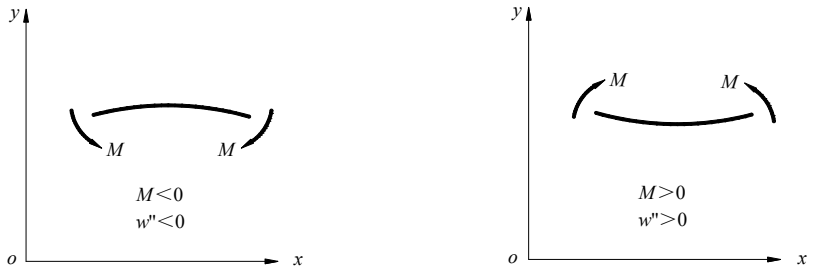
According to the principles of material mechanics, the relationship between bending moment and deflection at any cross-section of a beam segment can be expressed as:

$$\frac{1}{\rho(x)} = \frac{M(x)}{EI} \tag{8}$$

$$\frac{1}{\rho(x)} = \pm\frac{w''}{(1+w'^2)^{3/2}} \tag{9}$$

where w'' represents the second derivative of the beam deflection, E denotes the elastic modulus of the main girder, I is the sectional moment of inertia of the main girder, and $\rho(x)$ indicates the curvature at section x.

When the x-axis is defined as positive to the right and the y-axis as positive upward, a downward-convex curvature is positive, while an upward-convex curvature is negative. According to the sign convention for bending moments, a downward-convex bending moment is positive, and an upward-convex bending moment is negative, as illustrated in Figure 3. It is evident that under this coordinate system, the signs of M and w'' are consistent. Substituting Equation (9) into Equation (8) yields:



(a) Upward (b) Downward

Figure 3. Relationship between bending moment and second derivative in a local beam segment.

$$\frac{w''}{(1+w'^2)^{3/2}} = \frac{M(x)}{EI} \tag{10}$$

Since the deflection curve of the beam is relatively flat, w'^2 is extremely small compared to 1 and can be neglected. Thus, the above expression can be approximated as:

$$w'' = \frac{M(x)}{EI} \tag{11}$$

The second derivative of the deflection at a specific point on the main girder can be expressed using the second-order central difference formula as:

$$\frac{dw^2(x)}{dx^2} = \frac{w(x+\Delta x) - 2w(x) + w(x-\Delta x)}{(\Delta x)^2} \tag{12}$$

where $w(x-\Delta x), w(x), w(x+\Delta x)$ represent the deflection values at points $x-\Delta x, x, x+\Delta x$ on the main girder, respectively.

Substituting Equation (12) into Equation (11) yields:

$$M(x) = EI\frac{w(x+\Delta x) - 2w(x) + w(x-\Delta x)}{(\Delta x)^2} \tag{13}$$

2.1.2. Relationship Between Cable Force and Girder Deflection

(1) Undamaged cable condition

Consider a beam segment AB extracted from a long-span cable-stayed bridge, containing n stay cables. The anchorage points of these cables along the girder are sequentially numbered from left to right as 1, 2, …, $k-1$, k, $k+1$, …, m. The vertical components of

the cable forces are denoted as Y_1^h, Y_2^h, …, Y_{k-1}^h, Y_k^h, Y_{k+1}^h, …, Y_m^h, with a uniform spacing l between any two adjacent anchorage points. The distances from the left end of the beam segment to anchorage point 1 and from anchorage point n to the right end are denoted as l_a and l_b respectively.

The entire beam segment is subjected to a uniformly distributed load q. The bending moments and shear forces at ends A and B of segment AB are shown in Figure 4, which illustrates the undamaged cable condition.

In Figure 4, M_A^h and M_B^h represent the bending moments induced by all external loads at sections A and B, respectively, while Q_A^h and Q_B^h denote the corresponding shear forces caused by all external loads at sections A and B, respectively. The influence of axial forces is neglected. Under these conditions, the bending moments at points $k-1$, k and $k+1$ along the beam segment can be expressed as functions of the end forces, the uniformly distributed load q, and the vertical components of the cable forces.

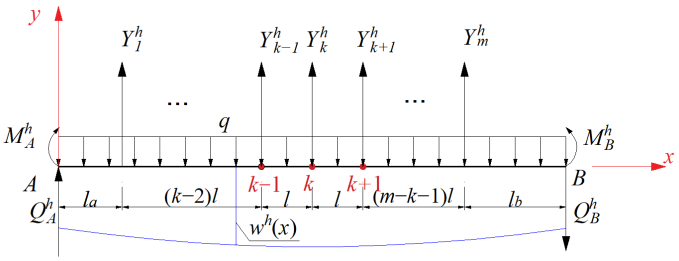


Figure 4. Force and deformation diagram of local beam segment (No cable damage).

According to Equation (7), parameter M^R under the undamaged condition can be expressed as:

$$M^{hR} = \frac{1}{2}ql^2 - \frac{1}{2}Y_k^h l \tag{14}$$

(2) Cable Damage Condition

Assume that the stay cable at an arbitrary point k on the girder experiences damage, as illustrated in Figure 5. The vertical components of the cable forces are denoted as Y_1^d, $\cdots$, Y_{k-1}^d, Y_k^d, Y_{k+1}^d, $\cdots$, Y_m^d, while M_A^d and M_B^d represent the bending moments induced by all external loads at sections A and B, respectively. Similarly, Q_A^d and Q_B^d denote the shear forces caused by all external loads at sections A and B, respectively.

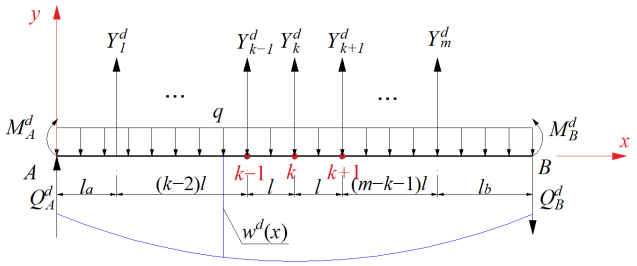


Figure 5. Force and deformation diagram of local beam segment (with cable damage).

According to Equation (7), M^R under the cable damage condition can be expressed as:

$$M^{dR} = \frac{1}{2}ql^2 - \frac{1}{2}Y_k^d l \tag{15}$$

Let:

$$\Delta Y_k = Y_k^d - Y_k^h \tag{16}$$

The variation (denoted as ΔM^R) in the bending moment M^R before and after the damage of cable k is given by:

$$\Delta M^R = M^{dR} - M^{hR} \tag{17}$$

Substituting Equations (14)–(16) into Equation (17) yields:

$$\Delta M^R = -\frac{1}{2} l \Delta Y_k \tag{18}$$

(3) Relationship Between Bending Moment and Deflection

Under undamaged cable conditions, the bending moment at any cross-section x can be expressed based on Equation (13) as:

$$M^h(x) = EI\frac{w^h(x+\Delta x) - 2w^h(x) + w^h(x-\Delta x)}{(\Delta x)^2} \tag{19}$$

where $w^h(x-\Delta x), w^h(x), w^h(x+\Delta x)$ and represent the deflection values at sections $x-\Delta x$, $x, x+\Delta x$ on the main girder under undamaged cable conditions, respectively; $M^h(x)$ denotes the bending moment at section x of the main girder when no cable damage is present.

Similarly, after the occurrence of cable damage, the bending moment at any section x can be expressed based on Equation (13) as:

$$M^d(x) = EI\frac{w^d(x+\Delta x) - 2w^d(x) + w^d(x-\Delta x)}{(\Delta x)^2} \tag{20}$$

where $w^d(x-\Delta x), w^d(x), w^d(x+\Delta x)$ represent the deflection values at sections $x-\Delta x$, $x, x+\Delta x$ on the main girder after cable damage occurs, respectively; $M^d(x)$ denotes the bending moment at section x of the main girder under cable damage conditions.

Let:

$$\begin{cases} \Delta w(x-\Delta x) = w^d(x-\Delta x) - w^h(x-\Delta x) \\ \Delta w(x) = w^d(x) - w^h(x) \\ \Delta w(x+\Delta x) = w^d(x+\Delta x) - w^h(x+\Delta x) \end{cases} \tag{21}$$

Therefore, the bending moment difference $\Delta M(x)$ at location x of the main girder before and after cable damage can be expressed as:

$$\Delta M(x) = M^d(x) - M^h(x) \tag{22}$$

Substituting Equations (19)–(21) into Equation (22) yields:

$$\Delta M(x) = EI\left(\frac{\Delta w(x+\Delta x) - 2\Delta w(x) + \Delta w(x-\Delta x)}{(\Delta x)^2}\right) = EI\Delta w''(x) \tag{23}$$

Under undamaged cable conditions, the bending moment M^R can be expressed based on Equation (2) as:

$$M^{hR} = M_k^h - \frac{1}{2}\left(M_{k-1}^h + M_{k+1}^h\right) \tag{24}$$

When cable damage occurs, the bending moment M^R can be expressed according to Equation (2) as:

$$M^{dR} = M_k^d - \frac{1}{2}\left(M_{k-1}^d + M_{k+1}^d\right) \tag{25}$$

Using Equations (24) and (25), parameter ΔM^R can be expressed as:

$$\begin{aligned}\Delta M^R &= \left(M_k^d - \tfrac{1}{2}\left(M_{k-1}^d + M_{k+1}^d\right)\right) - \left(M_k^h - \tfrac{1}{2}\left(M_{k-1}^h + M_{k+1}^h\right)\right) \\ &= \left(M_k^d - M_k^h\right) - \tfrac{1}{2}\left(\left(M_{k-1}^d - M_{k-1}^h\right) + \left(M_{k+1}^d - M_{k+1}^h\right)\right)\end{aligned} \tag{26}$$

Let:

$$\begin{cases}\Delta M_{k-1} = M_{k-1}^d - M_{k-1}^h \\ \Delta M_k = M_k^d - M_k^h \\ \Delta M_{k+1} = M_{k+1}^d - M_{k+1}^h\end{cases} \tag{27}$$

Substituting Equation (27) into Equation (26) yields:

$$\Delta M^R = \Delta M_k - \frac{1}{2}(\Delta M_{k-1} + \Delta M_{k+1}) \tag{28}$$

According to Equation (23), when x takes the values $k-1$, k, and $k+1$ respectively, the bending moment differences at sections $k-1$, k, and $k+1$ of the main girder can be expressed in terms of deflection differences as follows:

$$\begin{cases}\Delta M_{k-1} = EI\Delta w_{k-1}'' \\ \Delta M_k = EI\Delta w_k'' \\ \Delta M_{k+1} = EI\Delta w_{k+1}''\end{cases} \tag{29}$$

where $\Delta w_{k-1}''$, $\Delta w_k'$ and $\Delta w_{k+1}''$ represent the second derivatives of the beam deflection differences at sections $k-1$, k, and $k+1$, respectively.

Substituting Equation (29) into Equation (28) yields:

$$\Delta M^R = EI\left(\Delta w_k'' - \frac{1}{2}\left(\Delta w_{k-1}'' + \Delta w_{k+1}''\right)\right) \tag{30}$$

Comparing Equation (30) with Equation (18), it can be concluded that:

$$EI\left(\Delta w_k'' - \frac{1}{2}\left(\Delta w_{k-1}'' + \Delta w_{k+1}''\right)\right) = -\frac{1}{2}l\Delta Y_k \tag{31}$$

Using the forward difference formula, the second-order difference of the beam deflection can be expressed as:

$$\begin{cases}\Delta w_{k-1}'' = \frac{\Delta w_{k-1}(x+\Delta x) - 2\Delta w_{k-1}(x) + \Delta w_{k-1}(x-\Delta x)}{(\Delta x)^2} \\ \Delta w_k'' = \frac{\Delta w_k(x+\Delta x) - 2\Delta w_k(x) + \Delta w_k(x-\Delta x)}{(\Delta x)^2} \\ \Delta w_{k+1}'' = \frac{\Delta w_{k+1}(x+\Delta x) - 2\Delta w_{k+1}(x) + \Delta w_{k+1}(x-\Delta x)}{(\Delta x)^2}\end{cases} \tag{32}$$

Substituting Equation (32) into Equation (31) yields:

$$\begin{aligned}&EI\left(\frac{\Delta w_k(x+\Delta x) - 2\Delta w_k(x) + \Delta w_k(x-\Delta x)}{(\Delta x)^2}\right. \\ &-\frac{1}{2}\left(\frac{\Delta w_{k-1}(x+\Delta x) - 2\Delta w_{k-1}(x) + \Delta w_{k-1}(x-\Delta x)}{(\Delta x)^2}\right. \\ &\left.\left.+\frac{\Delta w_{k+1}(x+\Delta x) - 2\Delta w_{k+1}(x) + \Delta w_{k+1}(x-\Delta x)}{(\Delta x)^2}\right)\right) \\ &= -\tfrac{1}{2}l\Delta Y_k\end{aligned} \tag{33}$$

Furthermore,

$$\Delta Y_k = \Delta F_k \sin\alpha_k \tag{34}$$

where α_k defines the inclination of the cable tension relative to the deck girder.

Therefore,

$$\begin{aligned}\Delta F_k = & \\ & -2EI\left(\frac{\Delta w_k(x+\Delta x)-2\Delta w_k(x)+\Delta w_k(x-\Delta x)}{(\Delta x)^2}\right. \\ & -\frac{1}{2}\left(\frac{\Delta w_{k-1}(x+\Delta x)-2\Delta w_{k-1}(x)+\Delta w_{k-1}(x-\Delta x)}{(\Delta x)^2}\right. \\ & \left.\left.+\frac{\Delta w_{k+1}(x+\Delta x)-2\Delta w_{k+1}(x)+\Delta w_{k+1}(x-\Delta x)}{(\Delta x)^2}\right)\right)/(l\sin\alpha_k)\end{aligned} \tag{35}$$

From Equation (35), it can be observed that a specific relationship exists between the second-order deflection differences at points $k-1$, k, and $k+1$, and the variation in cable force at point k.

The damage index of second-order difference (DISOD) is defined as:

$$\begin{aligned}DISOD(k) = & \frac{\Delta w_k(x+\Delta x)-2\Delta w_k(x)+\Delta w_k(x-\Delta x)}{(\Delta x)^2} \\ & -\frac{1}{2}\left(\frac{\Delta w_{k-1}(x+\Delta x)-2\Delta w_{k-1}(x)+\Delta w_{k-1}(x-\Delta x)}{(\Delta x)^2}\right. \\ & \left.+\frac{\Delta w_{k+1}(x+\Delta x)-2\Delta w_{k+1}(x)+\Delta w_{k+1}(x-\Delta x)}{(\Delta x)^2}\right)\end{aligned} \tag{36}$$

When cable k experiences damage, its tension force decreases, resulting in a positive damage index. Otherwise, the damage index remains zero or negative. Therefore, by utilizing the deflection information from nine cross-sectional positions at three anchorage points $k-1$, k, and $k+1$ (as illustrated in Figure 6, it becomes feasible to determine whether cable k has sustained damage.

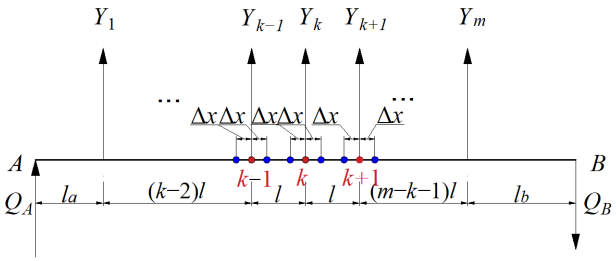


Figure 6. Schematic diagram of dense deflection data points required for calculating the damage index.

2.2. The Process of Identifying Cable Damage

This paper introduces a cable damage identification method that leverages the second-order difference of local beam deflection, tailored for cable-stayed bridge applications. See Figure 7.

The linear bridge profile under design conditions serves as the benchmark for pre-damage beam deflection at each anchorage point. For cable-stayed bridges lacking this reference data, an initial finite element model is first established using design parameters and initial cable forces. This model is then updated with field-measured data to create a reference finite element model. Finally, the bridge profile under self-weight is calculated from this corrected model to determine the main beam's initial deflection.

(1) Periodically measure the deflection at cable and main beam anchorage points (every quarter or year), thus capturing the beam deflection data after potential cable damage.
(2) Compute the deflection difference between the results of steps (2) and (1), forming the column vector of beam deflection differences.

(3) Encrypt the deflection difference data points obtained above and calculate the damage index DISOD(k) values at each cable position based on Equation (36). Evaluate whether the cable is damaged by considering the sign of the resulting value (positive or negative).

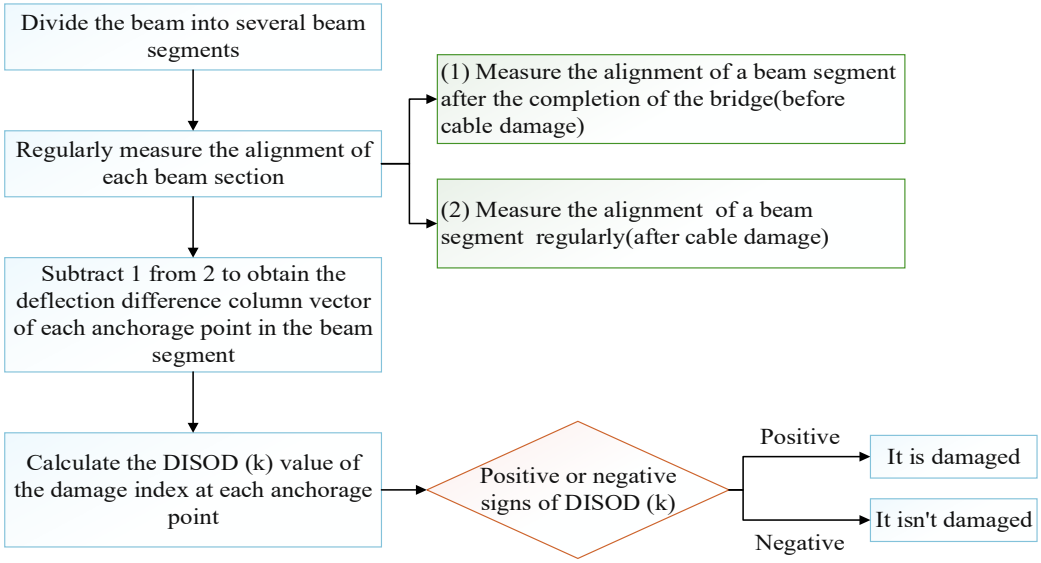


Figure 7. Procedure for locating damaged cables.

3. Field Bridge Simulation Analysis

3.1. Engineering Overview

This bridge is a double-tower, double-cable-plane prestressed concrete cable-stayed bridge. This bridge is built in 2010. The main bridge has a total length of 821 m with a span arrangement of (43 + 147 + 386 + 147 + 43) meters. It adopts a semi-floating structural system, with vertical supports provided at the auxiliary piers, transition piers, and the lower cross beams of the cable towers. To enhance overall stability, lateral wind-resistant bearings and longitudinal viscous dampers are installed at the cable tower locations, with specific arrangements shown in Figure 8.

The girder features a standard double-main-rib cross-section, with a full width of 27.5 m and a center girder height of 2.6 m. The top slab is 23.5 m wide and 0.30 m thick, with a 2.0% bidirectional cross slope on the bridge deck. The outer height of the ribs in the standard section is 2.33 m, with each rib being 2.0 m wide. In the side-span cast-in-place segments, the width of the main girder ribs transitions gradually from 2.0 m to 3.5 m. Detailed cross-sectional configurations are provided in Figure 9.

The standard sections of the main girder are constructed using the cantilever cast-in-place method with form travelers and are designed as prestressed concrete structures with a concrete strength grade of C60. A large cross beam, 300 cm thick, is provided at each cable tower and auxiliary pier, with all cross beams being prestressed concrete structures.

The cable towers are designed as “H”-shaped pylons, constructed as reinforced concrete structures with a total height of 193 m. The upper pylon segment is 78.5 m high, the middle segment is 42 m high, and the lower segment is 72.5 m high. The pylons are designed as prestressed reinforced concrete box sections.

The stay cables consist of parallel steel wire strands, formed by spirally bundling multiple layers of φ7 galvanized steel wires. They feature double-layer PE protection and are free of wire splices. The standard spacing of the stay cables on the main girder is 6 m, while the spacing in the cast-in-place sections of the side spans is 4.5 m. On the cable towers, the cable spacing is 1.75 m and 2.0 m, respectively.

A total of six types of stay cables are used for the entire bridge, namely PES7-85, PES7-109, PES7-139, PES7-151, PES7-187, and PES7-211.

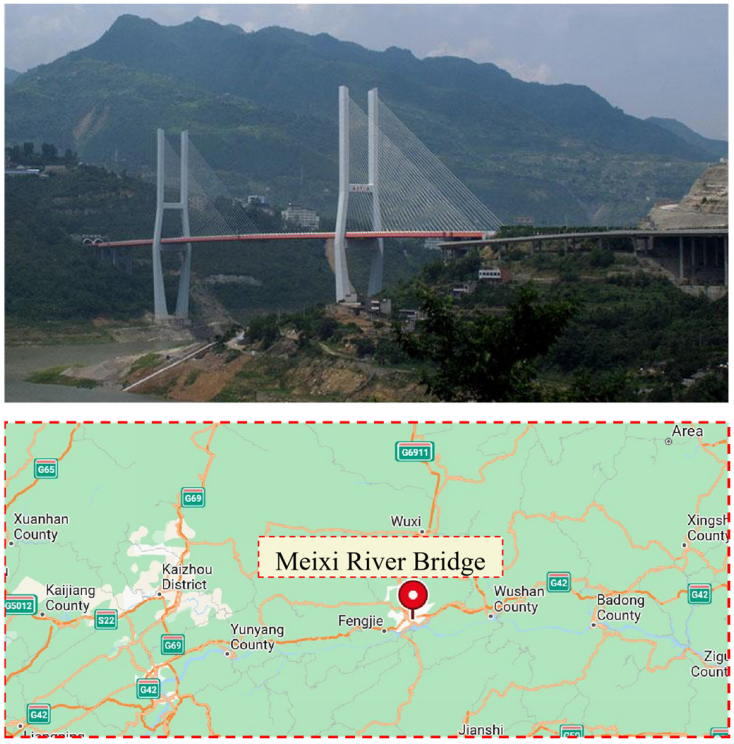
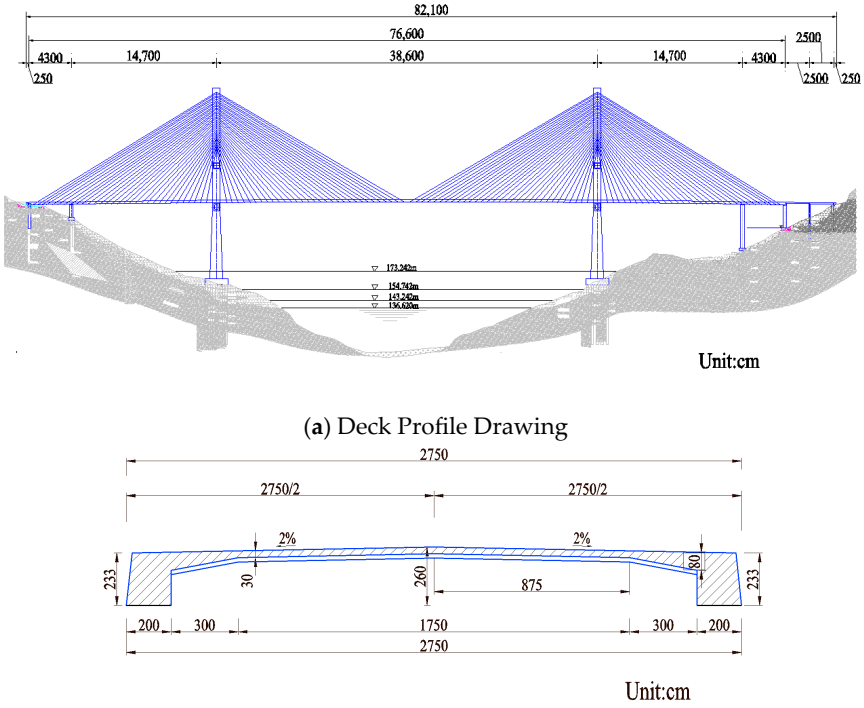


Figure 8. A practical large-span cable-stayed bridge with twin towers.



(**a**) Deck Profile Drawing

(**b**) Cross-Section Drawing

Figure 9. General Layout of the Bridge.

3.2. Development of the Numerical Model

A three-dimensional finite element model was constructed in ANSYS 19.2 [19] (see Figure 10). The fishbone beam modeling methodology was utilized to reduce the intricate

bridge deck system to a central spine beam featuring arranged stiffeners. This technique successfully optimizes the trade-off between processing demands and the fidelity necessary for comprehensive structural assessment. BEAM188, SOLID65, and LINK10 elements were assigned to the main beam, tower, and cables, respectively. The bottom of the main beam was constrained at the piers, and the second-phase dead load was simulated as a uniformly distributed load on the deck. The model comprises 1478 elements and 2137 nodes.

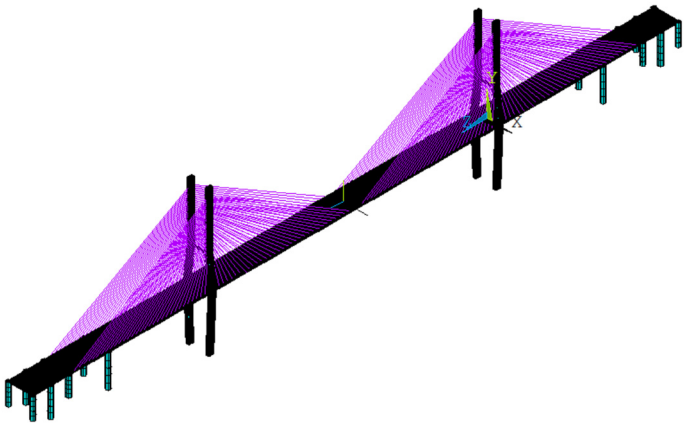


Figure 10. Finite element model of the twin towers cable-stayed bridge.

3.3. Cable Damage Location Identification

The loss of stiffness following cable damage is simulated via a reduction in the elastic modulus, corresponding to the method described in literature [20]. For a given cable i, the damage level $\aleph_i$ is calculated as

$$\aleph_i = 1 - \frac{E_{di}}{E_{ui}} \tag{37}$$

where E_{di} and E_{ui} are the elastic moduli of cable i after and before damage, respectively.

The damage identification begins with a rationally segmented main beam, where the deflection at each anchorage point is computed before and after single or double cable failure. Based on this data, the deflection and deflection difference relative to each segment's base point are calculated. Cable damage is then localized using the second-order difference principle of deflection on local beam segments. The mid-span, comprising 62 cables, is divided into six sections numbered 1 to 6 from left to right. Each section contains 14–15 cables and uses the left-end anchorage as its reference point, except for Section 1, which is referenced to point A1 at the bridge tower–girder connection. Adjacent local beam segments overlap by one internode (two cables), enabling clear damage localization across segments 1–6. The specific procedure is outlined in Figure 11.

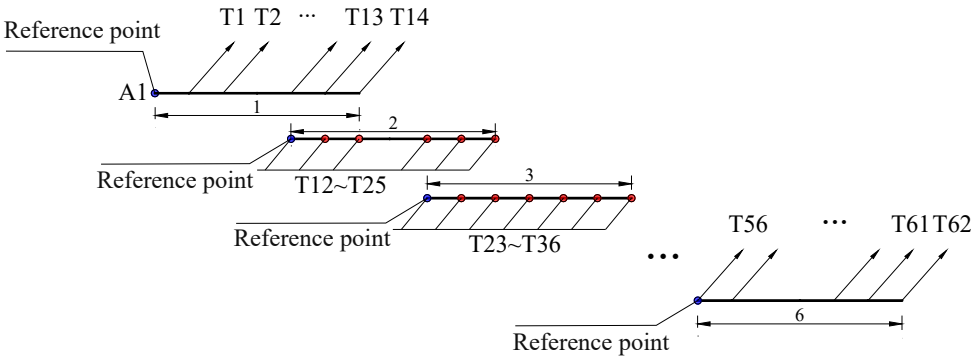


Figure 11. Schematic diagram of segmented identification of damaged cable positions.

(1) Single cable damage

Numerical simulations of cable damage are conducted at three representative locations (1/8, 1/4, and 1/2 span) to identify the damage position. Assuming single cables T8, T16, and T31 experienced damage levels of 10% to 40%, a finite element model computed the deflection differences $\Delta w(x)$ at anchorage points before $w^h(x)$ and after $w^d(x)$ damage, using the left-end anchorage point of the beam segment as the reference.

For instance, to simulate the failure of cable T31, a beam segment MN encompassing 14 cable spans (cables T25 to T38) is extracted, with its left-end anchorage point serving as the reference (Figure 12).

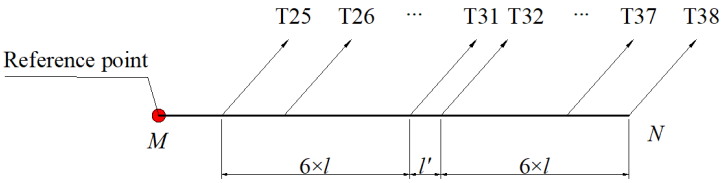


Figure 12. Part of beam section MN.

The damage index DISOD(k) is calculated using Equation (36), based on the second-order difference of the deflection at each anchorage point (from Equation (32)). The result is shown in Figure 13c.

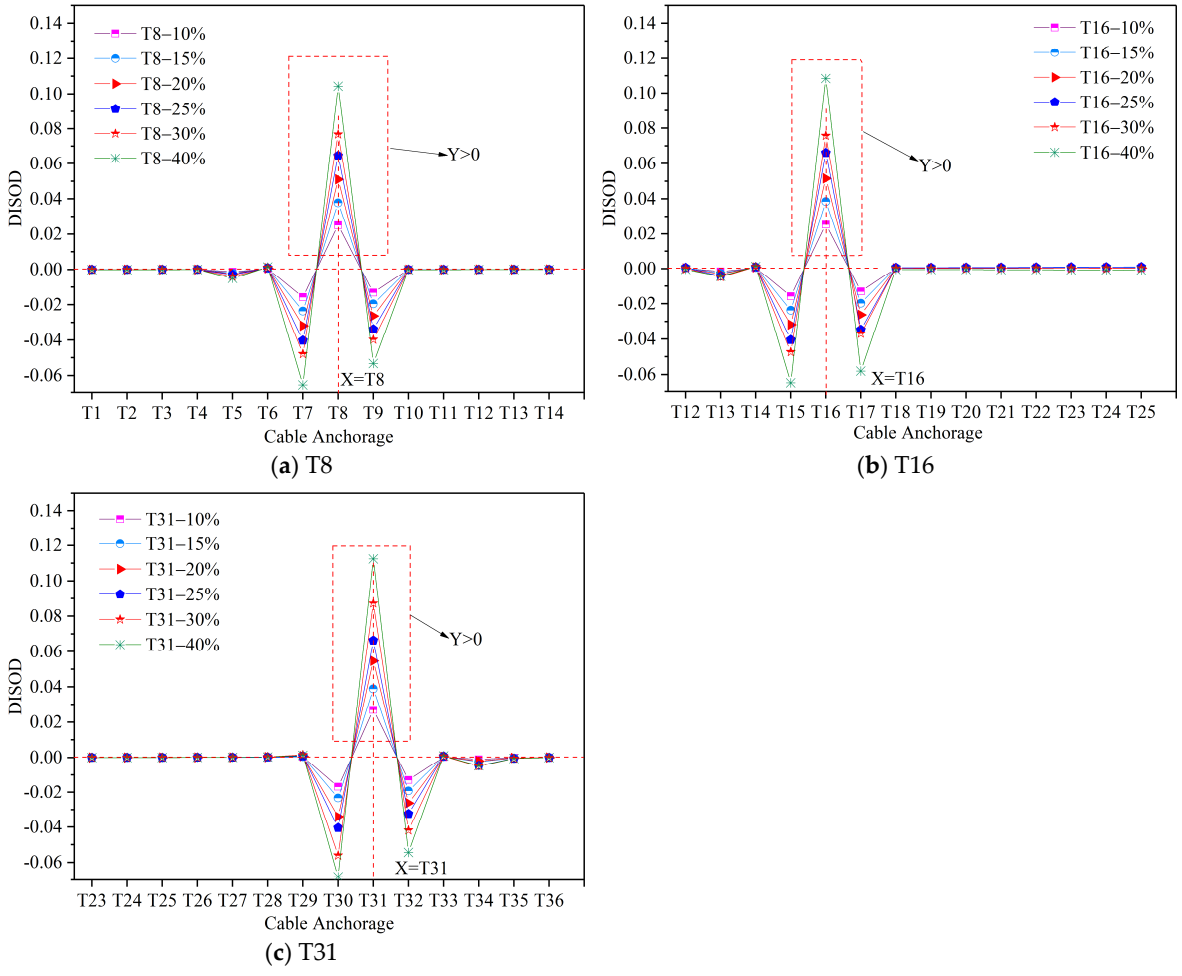


Figure 13. Calculation results of DISOD in case of single cable damage.

The locations of cable damage are simulated and identified at three positions (1/8 span position, 1/4 span position, 1/2 span position). Assuming different degrees of damage for single cables T8, T16, and T31 (10%, 15%, 20%, 25%, 30%, 40%), a finite element model of the double-tower cable-stayed bridge is developed to simulate anchorage point deflections $w^h(x)$ (before damage) and $w^d(x)$ (after damage), from which the beam deflection difference $\Delta w(x)$ is calculated. The damage index DISOD(k) is subsequently computed employing Equation (36).

Figure 13 presents the DISOD results under single cable damage conditions, comparing states before and after damage.

From Figure 13a, it can be seen that the damage index DISOD at the position of cable T8 is a positive value and reaches an extreme value, indicating a decrease in cable tension. The negative damage index DISOD measured at positions T7 and T9 corresponds to a rise in tensile force within these cables. A slight decrease in cable tension is reflected by the zero or negative DISOD values observed at the positions of other cables, which is in line with the pattern of cable tension changes after damage in cable, indicating that the damaged cable is cable T8. Furthermore, as the damage severity increases, the value of the damage index DISOD at the position of cable T8 increases.

Thus, it can be inferred that in Figure 13b,c, the damaged cables are T16 and T31 respectively, and the values of the damage index increase with the degree of damage.

(2) Double cable damage

Assuming varying degrees of damage to both cords (See Table 1). Follow the injury cord identification process proposed in the first section for cord location identification. Figures 14–16 show the DISOD calculation results for the cable damage conditions listed in Table 1.

Table 1. Damage conditions (Ansys simulation).

Damage Types	Position	Damage Conditions	Cable	Damage Degree (%)
Adjacent	1/8 Span	Case 1–Case 6	T8	5, 10, 15, 20, 30, 40
			T9	5, 10, 15, 20, 30, 40
	1/4 Span	Case 7–Case 12	T16	5, 10, 15, 20, 30, 40
			T17	5, 10, 15, 20, 30, 40
	1/2 Span	Case 13–Case 18	T31	5, 10, 15, 20, 30, 40
			T32	5, 10, 15, 20, 30, 40
Non-adjacent	1/8 Span	Case 19–Case 24	T8	5, 10, 15, 20, 30, 40
			T10	5, 10, 15, 20, 30, 40
		Case 25–Case 30	T8	5, 10, 15, 20, 30, 40
			T15	5, 10, 15, 20, 30, 40

Analysis of Figure 14a reveals that the distribution curve of the damage index DISOD shows positive values at the locations of cables T8 and T9, with relatively large numerical values. At the same time, the DISOD values at the locations of cables T7 and T10 sharply decrease. This reflects a decrease in the tension values of cables T8 and T9, while the tension values of cables T7 and T10 increase. Therefore, it can be concluded that cables T8 and T9 have sustained damage.

Similarly, by observing Figure 14b,c, it can be seen that the distribution curves of DISOD show positive values at the positions of cables T16&T17, and T31&T32, with negative values on their left and right sides, indicating damaged cables T16&T17, and T31&T32.

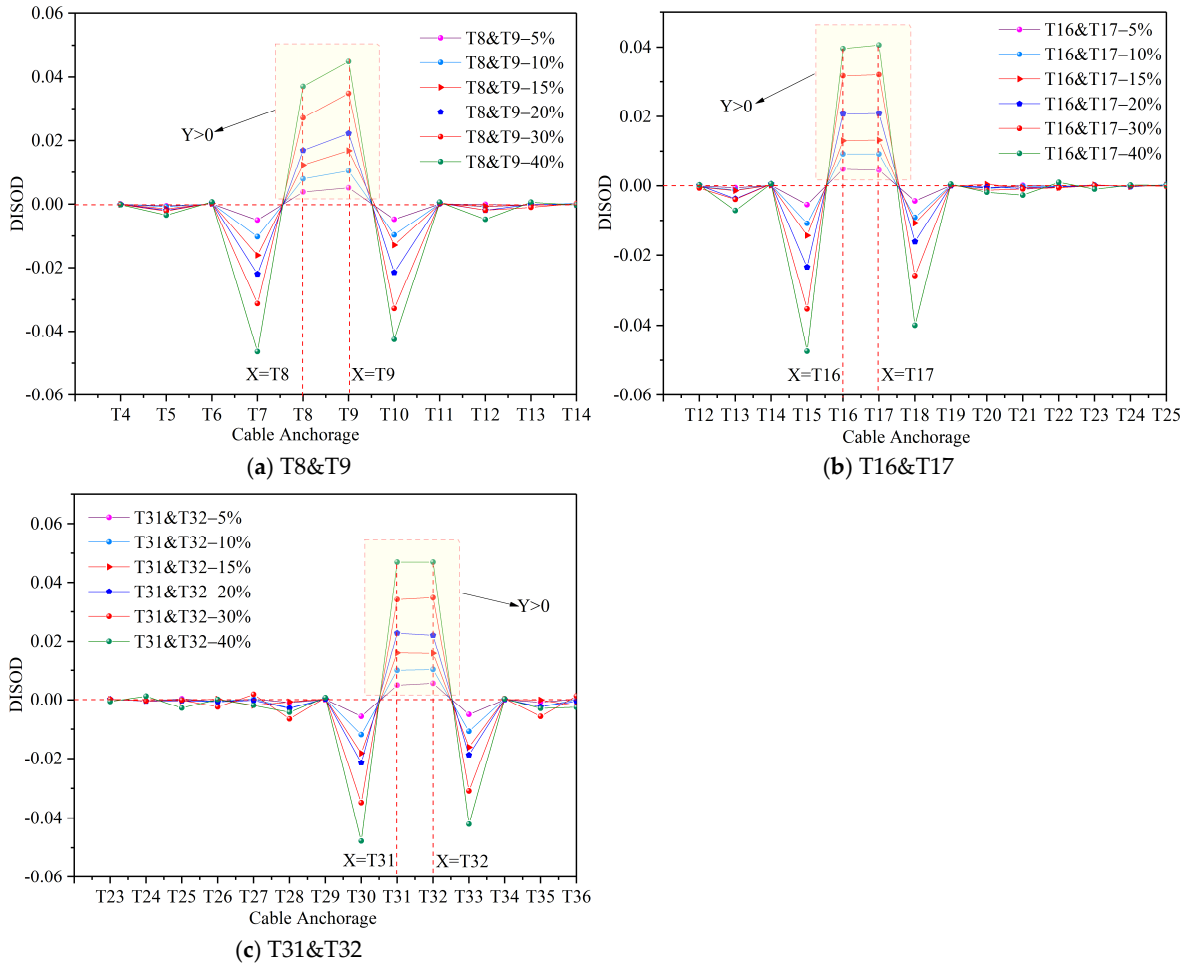


Figure 14. Calculation results of DISOD in case of adjacent cable damage.

For the case of non-adjacent double cable damage, taking the damage of cables T8 and T10 as an example, calculate the second-order difference in deflection of the beam segment at each anchorage point position on the first local beam segment at the left end of the main beam, and then use Equation (36) to calculate the value of the damage index DISOD (k). Following this method, starting from the end of the main beam, from left to right, calculate the damage index values of each anchorage point position on each local beam segment, and extract the cable force identification results of the cables on some local beam segments, as shown in Figure 15.

Figures 15 and 16 present the distribution curves of the damage index DISOD for the case of non-adjacent cable damage.

According to Figure 15, for non-adjacent cable injuries, the distribution curve of the damage index DISOD shows double positive peaks (extremum), and the peak value in the DISOD distribution curve corresponds to the location of the damaged cable. The identified position at T8&T10 thereby confirms the preset damage scenario, validating the method's accuracy.

Similarly, damage to other non-adjacent cables can be identified, and the results of identifying the location of the damaged cable are shown in Figure 16. According to Figure 16, the damaged cables are cables T8&T15, which is exactly the same as the predetermined damage situation. It can be seen that the second-order difference of the deflection of a local beam segment containing 7 cables can accurately identify whether the cables on the beam segment have been damaged.

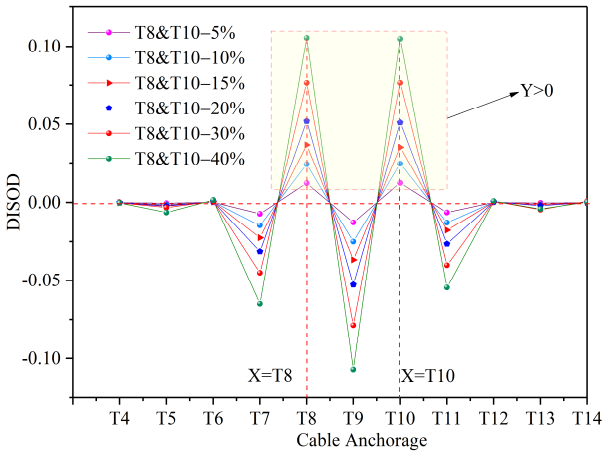
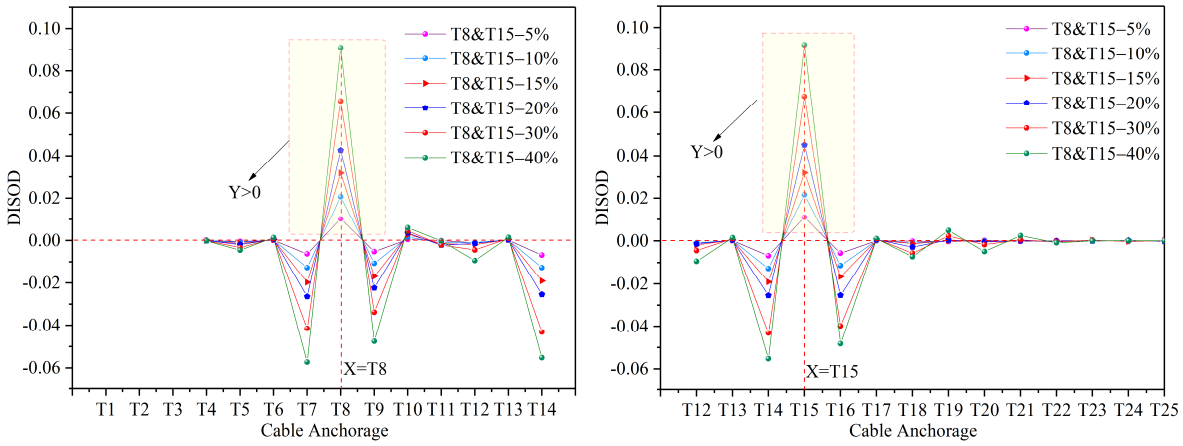


Figure 15. Calculation results of DISOD in case of non-adjacent cable damage (T8&T10).



(**a**) T1~T14 beam segment (**b**) T12~T25 beam segment

Figure 16. Calculation results of DISOD in case of non-adjacent cable damage (T8&T15).

4. Sensitivity Analysis of Damage Localization to Operational and Structural Factors

4.1. The Impact of Sampling Point Density on the Effectiveness of Damage Identification

The distribution curve of the beam deflection difference is derived from deflections measured at all cable-girder anchorage points before and after damage. Composed of discrete points spaced at 6 m intervals (the distance between main stay cables), this curve requires second-order differentiation for damage identification. According to calculus theory, the accuracy of this differentiation depends on the sampling point density. Consequently, the influence of sampling point quantity on identification accuracy must be considered.

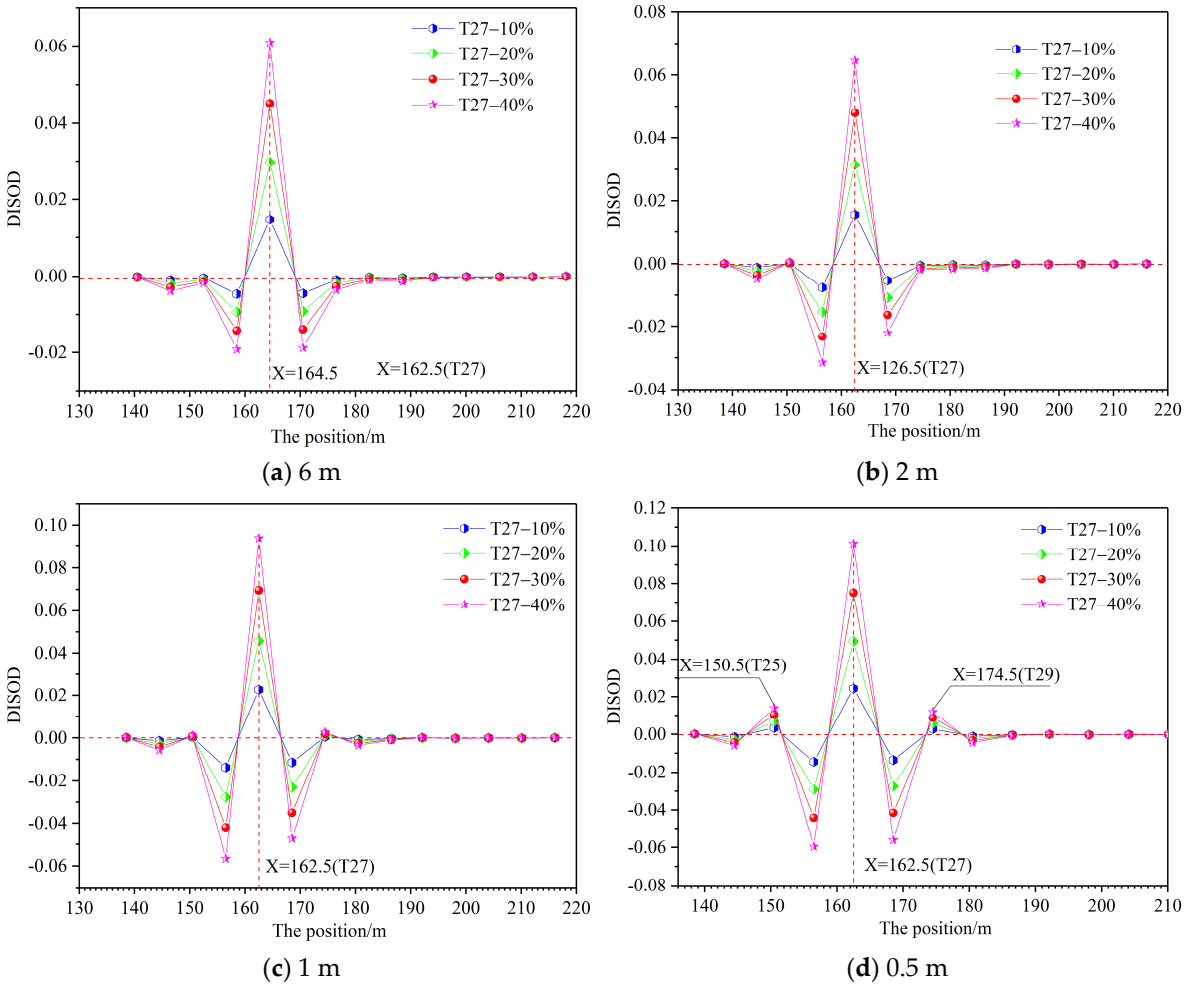
Table 2 provides the corresponding relationship between the stay cables and their positions on the main beam, providing position information for further analysis.

To analyze the influence of sampling point density on damage identification using the DISOD index, this study employed four sampling intervals (6 m to 0.1 m) for cable T27 with four damage severity levels (10–40%). The resulting DISOD values at each anchorage point are shown in Figure 16, illustrating the identification outcomes.

From Figure 17a–c, the damage index DISOD distribution curve shows a positive value at X = 162.5 m, with the damage index being T27, which is consistent with the preset damage index position.

Table 2. Location of cable anchorages on the main girder.

Cable No.	Distance/m	Cable No.	Distance/m	Cable No.	Distance/m	Cable No.	Distance/m
T1	6.5	T17	102.5	T33	198.1	T49	294.1
T2	12.5	T18	108.5	T34	204.1	T50	300.1
T3	18.5	T19	114.5	T35	210.1	T51	306.1
T4	24.5	T20	120.5	T36	216.1	T52	312.1
T5	30.5	T21	126.5	T37	222.1	T53	318.1
T6	36.5	T22	132.5	T38	228.1	T54	324.1
T7	42.5	T23	138.5	T39	234.1	T55	330.1
T8	48.5	T24	144.5	T40	240.1	T56	336.1
T9	54.5	T25	150.5	T41	246.1	T57	342.1
T10	60.5	T26	156.5	T42	252.1	T58	348.1
T11	66.5	T27	162.5	T43	258.1	T59	354.1
T12	72.5	T28	168.5	T44	264.1	T60	360.1
T13	78.5	T29	174.5	T45	270.1	T61	366.1
T14	84.5	T30	180.5	T46	276.1	T62	372.1
T15	90.5	T31	186.5	T47	282.1		
T16	96.5	T32	192.1	T48	288.1		



(**a**) 6 m (**b**) 2 m

(**c**) 1 m (**d**) 0.5 m

Figure 17. Effect of sampling point interval on damage identification accuracy.

From Figure 17d, it can be observed that when the number of sampling points increases to 0.5 m, the distribution curve of the second-order difference of local beam deflection (DISOD) features three prominent peaks., located at X = 150.5 m, X = 162.5 m, and X = 174.5 m, respectively. By referring to Table 2, it can be understood that these three local

maximum points correspond to cables T25, T27, and T29, namely the damage indices T25, T27, and T29. This situation leads to misjudgment compared to the preset situation of having only T27 as the damage index.

Therefore, the number of sampling points should be optimized, as excessive density can lead to misjudgment.

4.2. Assessing the Influence of Measurement Noise on Damage Identification Performance

The beam deflection data employed in Section 3 are synthetically generated via finite element simulation, contrasting with field-measured data in real-world applications. To evaluate the robustness of the cable damage identification method against various measurement disturbances, Gaussian white noise was introduced into the simulated deflection difference data prior to executing damage localization and severity assessment [10].

$$\Delta w_{noise} = \Delta w + RMS(\Delta w) \times \varepsilon_{level} \times \beta \tag{38}$$

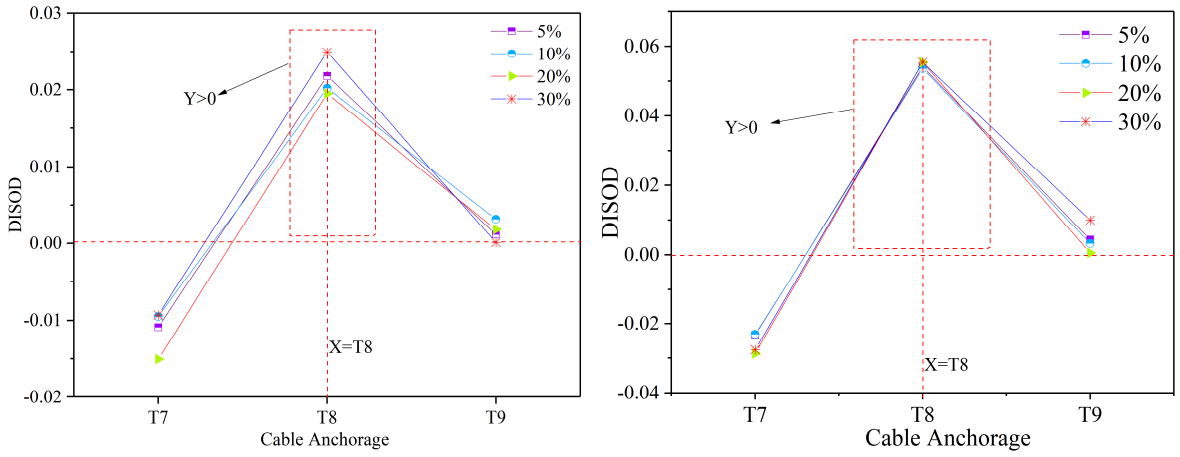
where Δw is the noise-free beam deflection difference, $RMS(\Delta w)$, ε_{level} and β are the root mean square (RMS) of Δw, the added noise level, and a standard normal random variable (mean = 0, variance = 1), respectively.

The table of working condition settings is shown in Table 3.

Table 3. Table of noise operating conditions.

Analysis Scenario	Case 1	Case 2	Case 3	Case 4
Introduced Measurement Noise	5%	10%	20%	30%

Using the data associated with the damage of cable T8 in Table 3, different levels of noise were added, and then the damage index value (DISOD) at each anchorage point position was calculated using Equation (36). The distribution curve of the damage index DISOD under different noise levels is obtained, as shown in Figure 18.



(**a**) T8 damage 10% (**b**) T8 damage 25%

Figure 18. Cable damage identification under different noise levels.

As illustrated in Figure 18, the damage index DISOD, derived from the second-order difference of local beam deflection, unambiguously identifies the damage at position X = T8. This identification is supported by a pronounced positive peak in its distribution, which persists consistently under measurement noise levels ranging from 10% to 40%. These findings collectively verify the method's precision in locating the preset damage and its strong resilience to noise.

4.3. Impact of Main Girder Stiffness Degradation on the Effectiveness of Damage Identification

The progressive deterioration of the main beam's global performance over the bridge's service life may compromise the accuracy of the proposed cable damage identification method. To account for this, beam degradation is simulated by reducing its flexural stiffness to 10%, 20%, 30%, and 40% of the original value.

To illustrate the methodology, a 30% damage at cable T8 is examined. The technique developed in Section 3, which relies on local beam deflection for damage localization, is employed to identify the compromised cable position. Figures 19 and 20 illustrate the investigation of the effect of main beam flexural stiffness degradation (main beam flexural stiffness degradation of 10%, 20%, 30%, 40%).

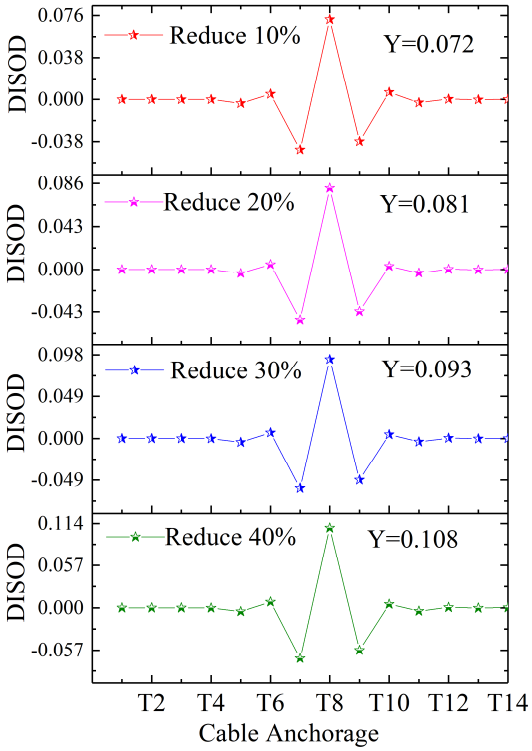


Figure 19. Performance of the DISOD method for damage identification under varying flexural stiffness conditions.

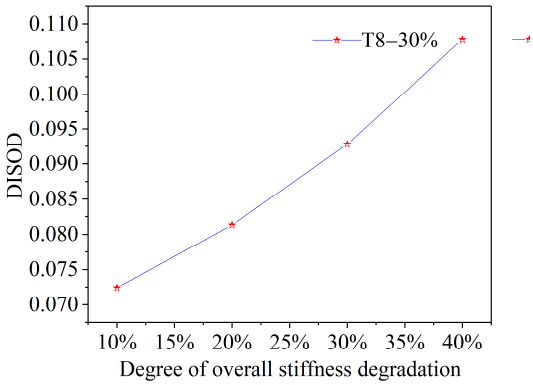


Figure 20. Variation in the DISOD damage index with main girder flexural stiffness.

Figure 19 presents results for different levels of main beam bending stiffness degradation (10%, 20%, 30%, 40%), the second-order difference of local beam deflection (DISOD) distribution curve always reaches a maximum at the position X = T8 before and after

different levels of damage occur to cable T8. The identified damage is precisely pinpointed at cable T8, which matches the intended preset location.

In Figure 20, as the bending stiffness of the main beam decreases, the peak value of the damaged cable with respect to the main beam anchorage point increases.

This study demonstrates that the degradation of the bridge's global stiffness improves the precision of damaged cable localization using the proposed second-order difference approach.

5. Assessment of a Cable Damage Identification Technique via a Scaled Laboratory Model

5.1. Description of the Experimental Model

To ensure a fair evaluation of the proposed method's advantages under consistent conditions, the experimental setup in this study utilizes the same scaled physical model originally developed and verified in our earlier work (Reference [17]). Prior validation has confirmed the model's consistent and reproducible structural behavior. Employing it as a controlled testbed minimizes variability introduced by model discrepancies, thereby attributing any performance differences directly to methodological improvements. This consistent experimental framework highlights the continuity of the research and supports an objective assessment of the enhanced capabilities of the present approach—particularly regarding noise robustness and accuracy in multi-damage localization—on a common and reliable basis.

(1) Design of Stay Cables

In this test model, the spacing between the stay cables in the side spans is 240 mm, while the spacing between the stay cables in the main span is 300 mm, totaling 20 pairs of stay cables. The stay cables are made of No. 15 steel wire ropes, which are composed of 7 strands of 3 mm diameter steel wires twisted together.

The lower end of each stay cable is connected to a cable damage simulation device, which consists of 9 springs of equal stiffness arranged in parallel. Additionally, each stay cable is connected in series with other related components, including an S-type tension sensor (capable of measuring the cable force) and a flange bolt (used to adjust the alignment of the girder and the cable force).

Each stay cable is configured in series with the following components: a steel wire rope connected to a tension meter, followed by hanging disks bracketing a spring assembly, and terminating at a flange and eyebolt connection.

This configuration ensures that the tensile stiffness of the cable is principally provided by the set of 9 parallel springs. The resulting deformation of the cable is thus manifested as the elongation or compression of these springs. By reducing the number of springs, varying degrees of cable damage can be accurately simulated. The mechanical response of the cable following damage is primarily governed by the deformation of its spring components, see Figure 21.

(2) Design of Counterweights

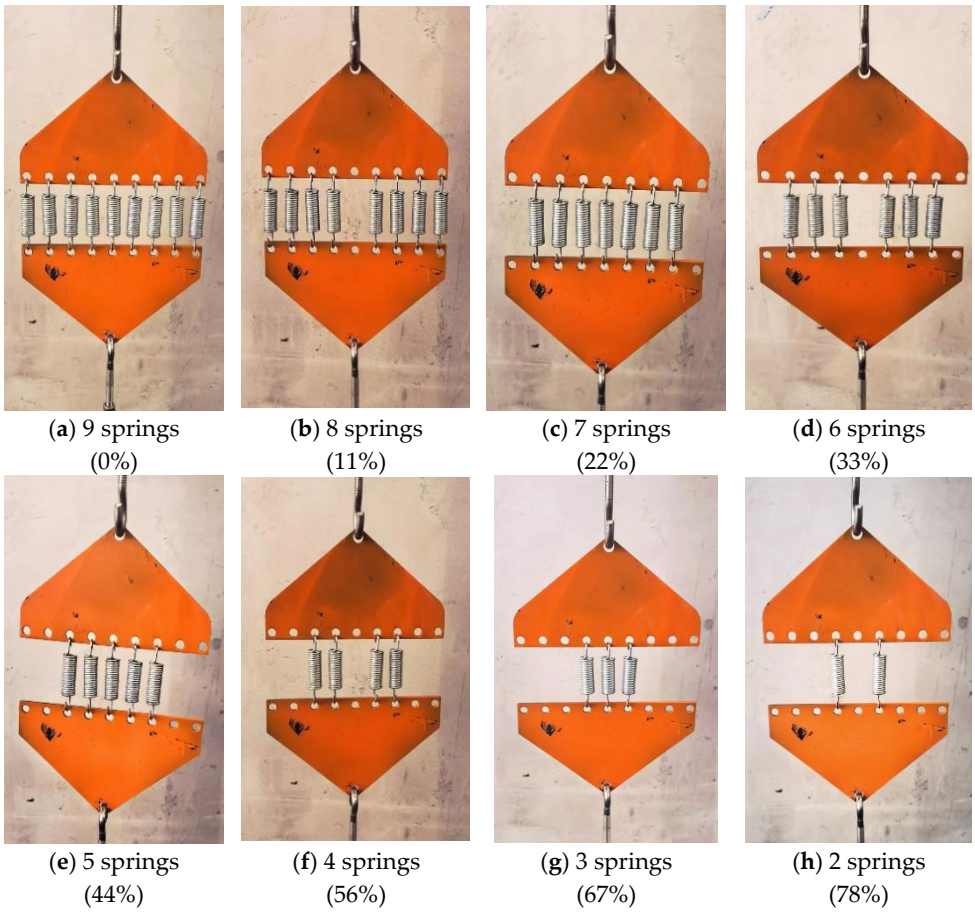
According to the similarity principle, to meet the requirements of dynamic similarity and ensure the measurability of deflections when simulating varying degrees of cable damage during the test, mass blocks are suspended on the crossbeams to increase the equivalent material density or equivalent unit weight of the test model.

The counterweight blocks are designed in two different thicknesses: one weighing 4.41 ± 0.5 kg and the other 8.83 ± 0.5 kg, as shown in Figure 22. These counterweights are distributed and concentrated on both sides of each crossbeam along the main girder in

a dispersed and concentrated loading manner. Wach suspension point carries a counterweight of 21.5 kg, with a total of 40 suspension points across the entire bridge, resulting in a total counterweight of 946 kg.

This method of dispersed and concentrated counterweight loading effectively simulates the stress state of the actual bridge under dead load and ensures accurate measurement of girder deflections when simulating varying degrees of cable damage during the test.

The physical installation of the counterweight loading method is shown in Figure 22.



(**a**) 9 springs (0%) (**b**) 8 springs (11%) (**c**) 7 springs (22%) (**d**) 6 springs (33%)

(**e**) 5 springs (44%) (**f**) 4 springs (56%) (**g**) 3 springs (67%) (**h**) 2 springs (78%)

Figure 21. Illustration of simulated damage degrees for stay cables.



Figure 22. Physical diagram of counterweight loading method.

(3) Model Design

A double-tower cable-stayed bridge model was designed based on the similarity ratio theory, with adjustments for site-specific constraints. The model's configuration (Figure 23)

has a total length of 6.68 m, a span arrangement of 1440 mm + 3300 mm + 1440 mm, a deck width of 600 mm, an overall height of 1.6 m, and pier heights of 0.56 m.

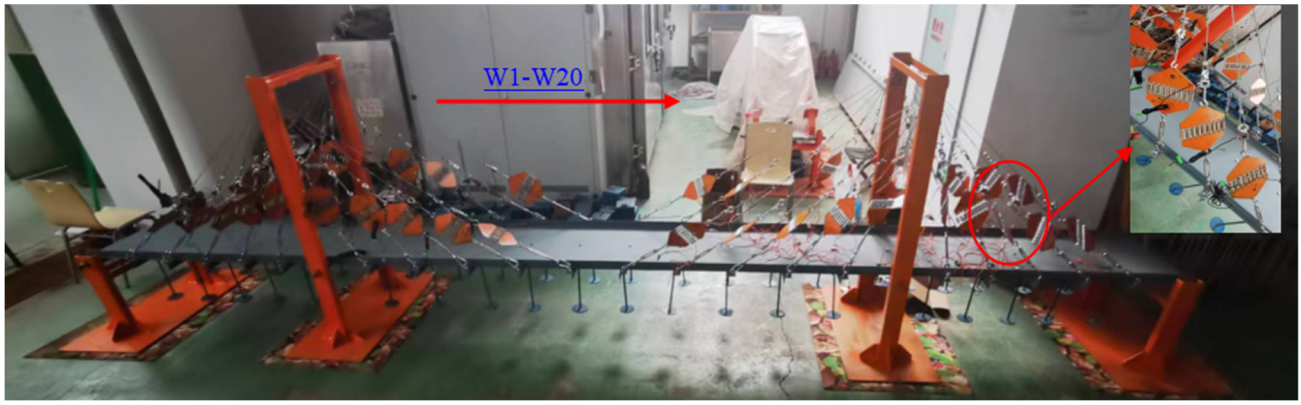


Figure 23. Experimental cable-stayed bridge model.

The model bridge was aligned in a north–south direction. The experimental setup was instrumented with 40 laser displacement transducers, all featuring a precision of 1 micron (0.001 mm). The sensors on the west side were designated as W1 to W20 (from south to north), as illustrated in Figure 24.

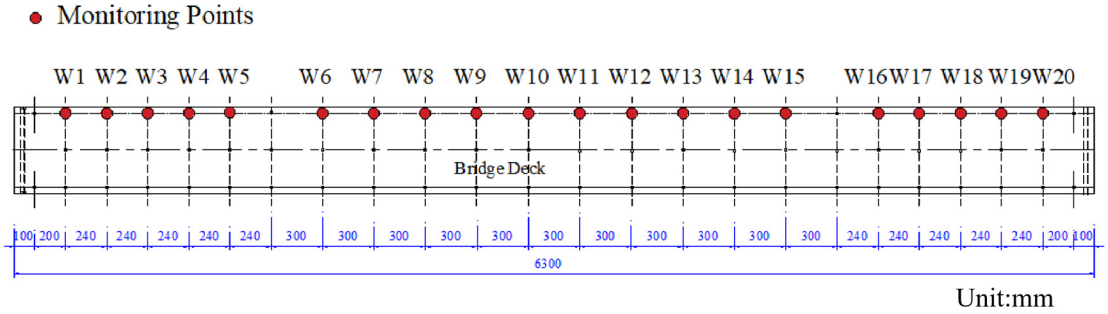


Figure 24. Sensor instrumentation layout.

(4) Assessment of Girder Deflection Induced by Cable Damage

The laser displacement sensor measures displacement based on the time taken for the laser to travel to and from the measured surface. During testing, the distance between the sensor and the measurement point is first adjusted to ensure that the vertical displacement of the girder remains within the sensor's measurement range and that valid readings are obtained throughout the process. Under the condition of undamaged stay cables, the cable-stayed bridge is adjusted to the designed alignment under its self-weight by tuning the cable forces and sensor positions. After the data stabilizes, the initial readings at each anchorage point are recorded (denoted as $w^h(x_i)$). Subsequently, damage to a specific stay cable is simulated (by gradually reducing the number of parallel springs), and once the sensor readings stabilize again, the final readings at each point are recorded (denoted as $w^d(x_i)$), See Figure 25.

The girder deflection difference Induced by cable damage Is defined by Equation (37):

$$\Delta w(x_i) = w^d(x_i) - w^h(x_i) \ (i = 1, 2, \ldots, n) \tag{39}$$

where the variable $\Delta w(x_i)$ is defined as the differential girder deflection observed at any given anchorage point, comparing pre-damage and post-damage states. The parameter n represents the total population of cable anchorage points on the girder structure.

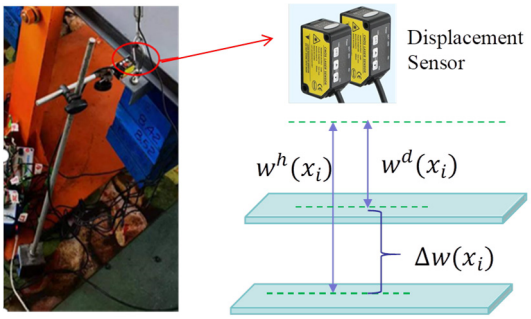


Figure 25. Schematic Diagram of Laser Displacement Sensor Installation and Measurement Principle.

5.2. Finite Element Modeling and Validation

A finite element model of the twin-tower cable-stayed bridge was developed in ANSYS based on the dimensions specified in Figure 26. The main girder, towers, and piers were modeled using BEAM188 elements with the properties of Q235 steel (elastic modulus $E = 2.00 \times 10^5$ Mpa). The bridge deck load was simulated by MASS21 elements uniformly distributed on the girder nodes. The completed model, shown in Figure 26, comprises 839 nodes and 594 elements.

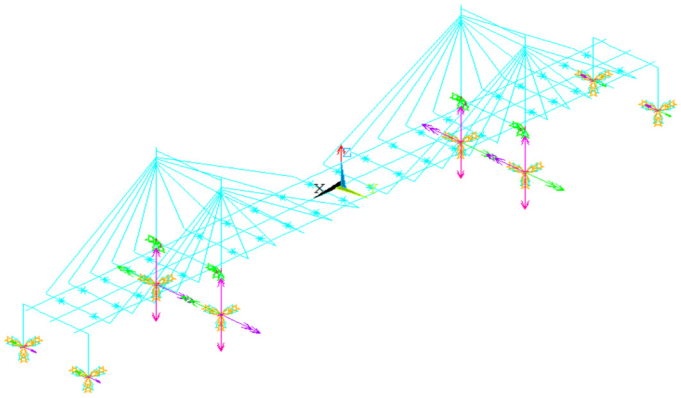


Figure 26. ANSYS model of the experimental bridge.

A benchmark finite element model was established by applying the designed initial cable forces (see values for W-1 to W-10) symmetrically across both towers, resulting in the intended initial girder profile. The close correlation between the measured and numerically simulated cable forces, presented in Figure 27, validates the model's accuracy, allowing it to serve as a reliable baseline for subsequent analysis.

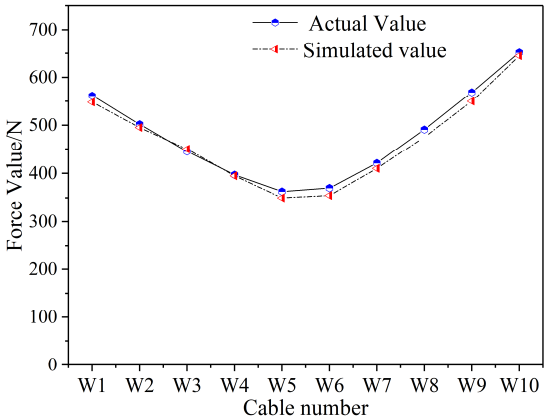


Figure 27. Comparison of experimental tensile Force and numerical simulation values.

5.3. Verification of the Method for Damaged Cable Localization

The experimental program comprised 32 working conditions, including scenarios of both single- and double-cable damage. Simulations of single-cable damage were conducted on cables W6 through W9 by removing 1 to 4 springs, respectively, to represent varying degrees of damage severity. The double-cable damage scenarios are summarized in Table 4.

Table 4. Damage conditions (Physical scale model test).

Damage Conditions		Cable No.	Extent of Damage (%)
Single Cable	MDC1-MDC4	W6	7, 20, 31, 48
	MDC5-MDC8	W7	10, 19, 29, 43
	MDC7-MDC12	W8	11, 23, 31, 45
	MDC13-MDC16	W9	12, 20, 34, 43
Double Cable	MDC17-MDC20	W6	7, 20, 31, 48
		W7	10, 19, 29, 43
	MDC21-MDC24	W6	7, 20, 31, 48
		W8	11, 23, 31, 45
	MDC25-MDC28	W6	7, 20, 31, 48
		W9	12, 20, 34, 43
	MDC29-MDC32	W8	11, 23, 31, 45
		W13	11, 23, 31, 45

The identification procedure commenced with the measurement of the deflection difference between cables and girder anchorages under each working condition listed in Table 4, yielding a deflection difference column vector. Subsequently, these data points were computationally encrypted using MATLAB2025a and processed through Equation (36) to generate the DISOD damage index distribution. The locations of damaged cables were determined by analyzing the peaks or anomalies in this distribution curve.

The calculation results of the damage Index DISOD for single and double cable damaged conditions are presented in Figures 28 and 29, respectively.

Figure 28a shows that for a single damaged cable, a positive DISOD value at position W6 indicates tension reduction, whereas negative values at W5 and W7 reflect tension redistribution. Thus, cable W6 is identified as damaged.

Similarly, based on Figure 28b–d, the damaged cables are determined to be W7, W8, and W9 respectively.

As shown in Figure 29a, after adjacent cables W6 and W7 were damaged, their DISOD values became positive, while the surrounding cables showed zero or negative values, accurately indicating that W6 and W7 were the damaged cables, which is consistent with the preset damage scenario.

Figure 29b demonstrates that when non-adjacent cables W6 and W8 were damaged, their DISOD values also turned positive, with neighboring cables exhibiting zero or negative values, again correctly identifying the damaged cables and matching the predefined damage conditions.

Similarly, Figure 29c,d confirm that the method successfully identified non-adjacent damaged cable pairs W6&W9 and W8&W13, respectively, based on the same DISOD criterion.

In conclusion, the DISOD method, interpreted through the sign of its values, has been demonstrated to be an effective tool for identifying damaged cables, whether single, adjacent, or non-adjacent.

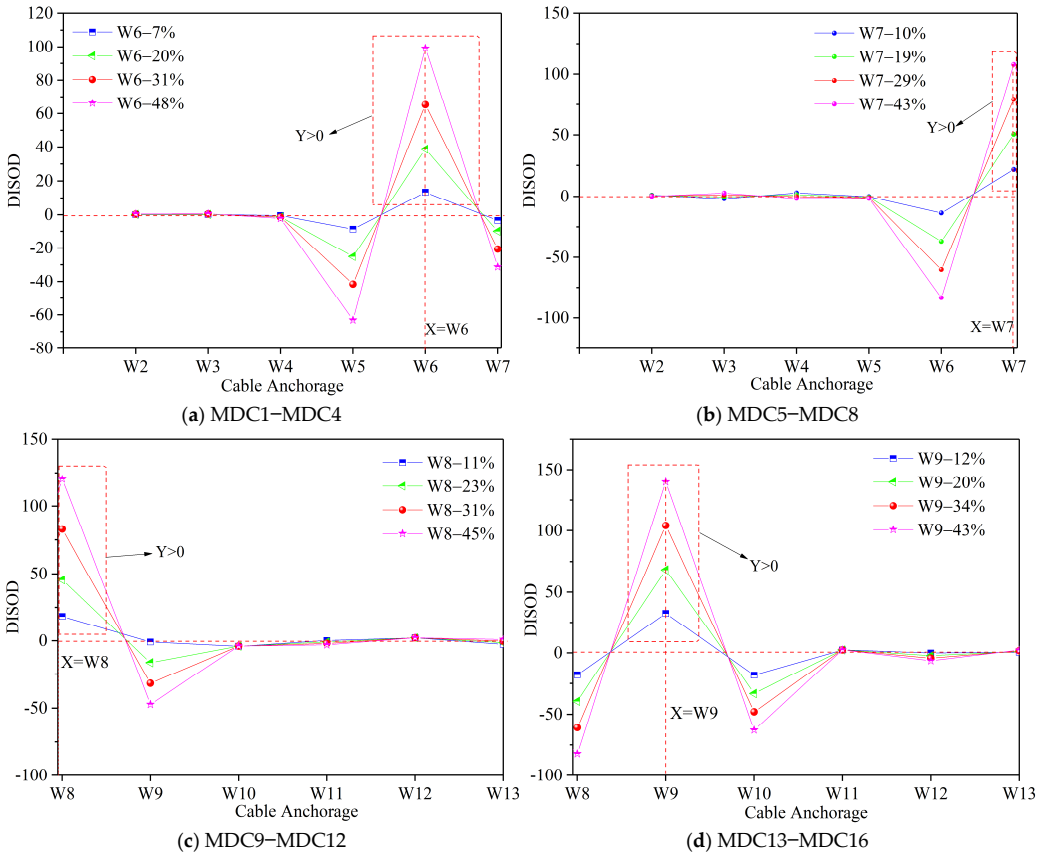


Figure 28. Identification results for single-cable damage.

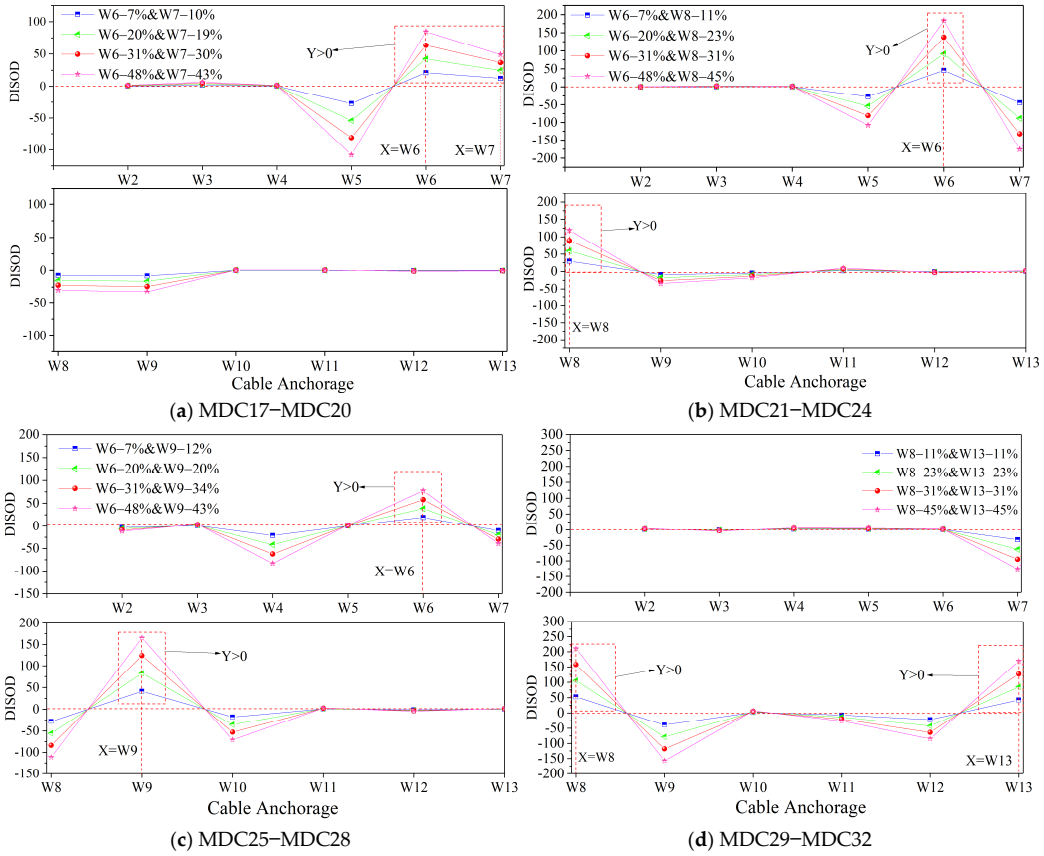


Figure 29. Identification results for double-cable damage.

6. Discussion

This study proposes a damage detection method for stay cables in cable-stayed bridges, which utilizes the second-order difference of local beam deflection. The method can accurately identify damaged cables by using only the deflection differences measured at three adjacent cable-girder anchorage points. Compared with the method in Reference [17], the proposed approach exhibits the following significant advantages:

(1) Simplified detection units: Damage identification can be achieved using measurement data from only three cables, significantly reducing reliance on the scale of sensor deployment and the precision of synchronous measurements.
(2) Enhanced computational efficiency: It eliminates the need to calculate the structural flexibility matrix under unit loads, substantially reducing computational effort.
(3) Improved engineering applicability: The method features a straightforward procedure and minimal parameter requirements, making it easier to integrate and implement in real bridge monitoring systems and thus offering greater potential for practical engineering applications.

7. Conclusions

This study presents a damage detection method for stay cables in cable-stayed bridges based on the second-order difference of local beam deflection. The proposed approach requires only the deflection differences from three adjacent cable-girder anchorage points to accurately locate damaged cables. Its reliability was validated through indoor model experiments, yielding the following conclusions:

(1) A damage index (DISOD) is established by correlating the second-order difference of deflections at three adjacent cable-girder anchorage points with the force variation in the middle cable. A positive DISOD value indicates damage in the middle cable, while a zero or negative value suggests the cable remains intact.
(2) The identification accuracy is influenced by the sampling point density, with a 1-m interval yielding optimal performance.
(3) The proposed method is robust to noise, demonstrating strong anti-interference capabilities and broad application potential.
(4) The accuracy of the proposed method improves as the overall structural performance degrades.

The DISOD indicator proposed in this study represents a paradigm shift from "direct cable force measurement" to "indirect deflection perception," effectively addressing engineering challenges such as the high cost and poor stability of traditional force sensors. Compared to existing dynamic monitoring methods, this technique demonstrates superior robustness against environmental interference and eliminates the need for establishing complex load–response mapping models.

The core limitation of this method lies in the strong coupling interference of multiple physical fields (temperature, adjacent cables, overall displacement, and wind-induced vibrations) within the deflection signal, making high-fidelity decoupling a persistent challenge. Future research will focus on developing a multi-modal fusion sensing system. By leveraging the technical complementarity and cross-validation of visual perception, millimeter-wave radar, and optical fiber sensing, a highly robust monitoring system with self-calibration capabilities will be constructed.

Author Contributions: Y.Y.: Conceptualization, Investigation, Writing—Original Draft. L.L.: Methodology, Investigation. S.L.: Conceptualization, Resources, Supervision, Writing—Review & Editing. L.Z.: Methodology, Validation, Writing—Review & Editing. H.X.: Resources, Supervision, Funding Acquisition. W.Y.: Software, Data Curation. S.Z.: Formal Analysis, Visualization. M.W.: Valida-

tion, Writing—Review & Editing. All authors have read and agreed to the published version of the manuscript.

Funding: This research was funded by the National Key R&D Program of China (Grant No. 2022YFB2603300) and the Shenzhen Science and Technology Program (Grant Nos. JCYJ20220818095608018, JCYJ20240813143211014). The APC was funded by Yanxiao Yang.

Institutional Review Board Statement: Not applicable.

Informed Consent Statement: Not applicable.

Data Availability Statement: All data are available within the article.

Acknowledgments: All acknowledged individuals have provided explicit consent for the mention of their names/contributions in this section.

Conflicts of Interest: Author Weile Yang was employed by the company China First Highway Engineering Co., LTD. Author Shaopeng Zhang was employed by the company Civil Engineering Design Research Institute, China Railway Design Corporation. Author Meng Wang was employed by the company Hebei Coal Science Research Institute Co., Ltd. The remaining authors declare that the research was conducted in the absence of any commercial or financial relationships that could be construed as a potential conflict of interest.

References

1. Pang, Y.; Wei, K.; He, H.; Wang, W. Assessment of lifetime seismic resilience of a long-span cable-stayed bridge exposed to structural corrosion. *Soil Dyn. Earthq. Eng.* **2022**, *157*, 107275. [CrossRef]
2. Iordachescu, M.; Valiente, A.; De Abreu, M. Effect of environmentally assisted damage on fatigue resistance of tie-down cables after 30 years of service in a cable-stayed bridge. *Eng. Fail. Anal.* **2021**, *126*, 105455. [CrossRef]
3. Lu, W.; He, Z. Vulnerability and robustness of corroded large-span cable-stayed bridges under marine environment. *J. Perform. Constr. Facil.* **2016**, *30*, 04014204. [CrossRef]
4. Ho, H.N.; Kim, K.D.; Park, Y.S.; Lee, J.J. An efficient image-based damage detection for cable surface in cable-stayed bridges. *Ndt E Int.* **2013**, *58*, 18–23. [CrossRef]
5. Zhong, J.W.; Wang, B.; Wang, X.; Wang, Z. Research and Application of Bridge Intelligent Detection Technology. *Bridge Constr.* **2019**, *49*, 1–6.
6. Xu, F.; Wang, X.; Wu, H. Inspection method of cable-stayed bridge using magnetic flux leakage detection: Principle, sensor design, and signal processing. *J. Mech. Sci. Technol.* **2012**, *26*, 661–669. [CrossRef]
7. Park, S.; Kim, J.W.; Lee, C.; Lee, J.; Gil, H.B. Local fault detection technique for steel cable using multi-channel magnetic flux leakage sensor. *J. Comput. Struct. Eng. Inst. Korea* **2012**, *25*, 287–292. [CrossRef]
8. Zhang, H.; Li, H.; Zhou, J.; Tong, K.; Xia, R. A multi-dimensional evaluation of wire breakage in bridge cable based on self-magnetic flux leakage signals. *J. Magn. Magn. Mater.* **2023**, *566*, 170321. [CrossRef]
9. Lepidi, M.; Gattulli, V.; Vestroni, F. Damage identification in elastic suspended cables through frequency measurement. *J. Vib. Control* **2009**, *15*, 867–896. [CrossRef]
10. Ko, J.M.; Sun, Z.G.; Ni, Y.Q. Multi-stage identification scheme for detecting damage in cable-stayed Kap Shui Mun Bridge. *Eng. Struct.* **2002**, *24*, 857–868. [CrossRef]
11. An, Y.; Chatzi, E.; Sim, S.H.; Laflamme, S.; Blachowski, B.; Ou, J. Recent progress and future trends on damage identification methods for bridge structures. *Struct. Control Health Monit.* **2019**, *26*, e2416. [CrossRef]
12. Ding, Y.; Li, A.; Du, D.; Liu, T. Multi-scale damage analysis for a steel box beam of a long-span cable-stayed bridge. *Struct. Infrastruct. Eng.* **2010**, *6*, 725–739. [CrossRef]
13. Catbas, F.; Gel, M.; Burkett, J. Damage assessment using flexibility and flexibility-based curvature for structural health monitoring. *Smart Mater. Struct.* **2007**, *17*, 015024. [CrossRef]
14. Tan, D.; Yao, H.; Chen, F.; Wu, H. Research on Damage Identification of Cable Damage in Cable-Stayed Bridges Based on Temperature Deflection. *J. Vib. Shock.* **2021**, *40*, 166−174. [CrossRef]
15. Wang, W.; Su, M.; Wang, C. Static Deflection Difference-Based Damage Identification of Hanger in Arch Bridges. *KSCW J. Civ. Eng.* **2022**, *26*, 5096–5106. [CrossRef]
16. Wang, W.; Su, M. Damage Identification in Hangers of Through-Arch Bridges Esing Static Deflection Difference at the Anchorage Point. *Appl. Sci.* **2021**, *11*, 10780. [CrossRef]

17. Yang, Y.; Su, M.; Li, W. Method for identifying damage to stay cables based on local beam deflection. *Phys. Scr.* **2024**, *100*, 015021. [CrossRef]
18. Shao, J. Real-time Quantitative Evaluation Method for Cable Damage of Cable-stayed Bridges Based on Abnormal Static Deflection Changes. Master's Thesis, China University of Mining and Technology, Beijing, China, 2022.
19. Ravichandran, G. *Finite Wlement Analysis of Weld Thermal Cycles Using ANSYS*; CRC Press: Boca Raton, FL, USA, 2020.
20. Ge, J.Y.; Su, M.B. Simulation Method for Cable Damage of Cable-Stayed Bridge and Its Effect on Cable Tension and Deflection Distribution. *China Railw. Sci.* **2016**, *37*, 30–37.

Disclaimer/Publisher's Note: The statements, opinions and data contained in all publications are solely those of the individual author(s) and contributor(s) and not of MDPI and/or the editor(s). MDPI and/or the editor(s) disclaim responsibility for any injury to people or property resulting from any ideas, methods, instructions or products referred to in the content.